Supporting Information

Single-isomer bis(pyrrolidino)fullerenes as electron transport materials for tin halide perovskite solar cells

Tomoya Nakamura,*[a] Takabumi Nagai,[b] Yuki Miyake,[a] Takumi Yamada,[a] Makoto Miura,[c] Hiroyuki Yosida,[c,d] Yoshihiko Kanemitsu,[a] Minh Anh Truong,[a] Richard Murdey,[a] Atsushi Wakamiya*[a]

[a.] Institute for Chemical Research, Kyoto University, Gokasho, Uji, Kyoto 611-0011, Japan
[b.] HARVES Co., Ltd., Saitama 330-0061, Japan
[c.] Graduate School of Engineering, Chiba University, Chiba 263-8522, Japan
[d.] Molecular Chirality Research Center, Chiba University, Chiba 263-8522, Japan

*E-mail: tomoya@scl.kyoto-u.ac.jp, wakamiya@scl.kyoto-u.ac.jp

Materials:

Formamidinium iodide (FAI, 99.99%, trace metal basis), methylammonium iodide (MAI, 99%, low water content), and bathocuproine (BCP, 99%, purified by sublimation) were purchased from Tokyo Chemical Industry Co., Ltd. (TCI). 2-Phenylethylammonium iodide (PEAI, 98%), tin(II) fluoride (SnF_2, 99%), tin(II) iodide (SnI_2, 99.99%, trace metal basis), and tin powder (<45 μm particle size, 99.8% trace metals basis) were purchased from Sigma-Aldrich Co., Ltd. (Sigma-Aldrich). Poly(3,4-ethylenedioxythiophene):poly (styrene sulfonate) (PEDOT:PSS) aqueous solution (Clevios P VP AI 4083) was purchased from Heraeus Co., Ltd. Phenyl-C_{61}-butyric acid methyl ester (**PCBM**) and indene-C_{60} bisadduct (**ICBA**) was purchased from Ossila. Dehydrated dimethylsulfoxide (DMSO, super dehydrated) was purchased from FUJIFILM Wako Pure Chemical Co., Ltd. Dimethylformamide (DMF) and chlorobenzene were purchased from Kanto Chemical. Co., Inc. All of these solvents were degassed by Ar gas bubbling for 1 h and further dried over molecular sieves (3 Å) in an Ar-filled glove box (O_2 < 0.1 ppm) before use. Fullerene C_{60} (99.5%) for synthesis was purchased from SES Research Inc. 2-(Phenylamino)octanoic acid[1] and *N*-(2-ethylhexyl)glycine[2] were synthesized according to the literature. Unless otherwise noted, materials purchased from commercial suppliers were used without further purification.

Computation method:

All calculations were conducted using the Gaussian 16 program.[3] The geometries were optimized at the B3LYP/6-31G(d) level of theory. The fact that these geometries are at the energy minimum was confirmed by frequency calculations at the same level of theory.

Perovskite layer fabrication:

0.8 M $PEA_{0.15}FA_{0.85}SnI_3$ perovskite precursor solution was prepared by dissolving PEAI (60 mg, 0.24 mmol), FAI (234 mg, 1.36 mmol), SnI_2 (596 mg, 1.60 mmol), SnF_2 (19 mg, 0.12 mmol), and tin powder (30 mg) in a mixed solvent of 1.6 mL DMF and 0.4 mL DMSO. The precursor solution was stirred at 70 °C for 1 h and filtered through a 0.20 μm PTFE filter before spin-coating. After the precursor solution was cooled down to room temperature, 100 μL of the precursor solution was spin-coated at 5000 rpm for 50 s with an acceleration of 1000 rpm s^{-1} (total time for spin-coating is 55 s). 500 μL of toluene antisolvent was dripped onto the surface of the spinning substrate at 52 s during the spinning. Then, the substrate was immediately annealed on a 70 °C hot plate for 10 min. All the steps above were conducted in an Ar-filled glove box (H_2O, O_2 < 0.1 ppm).

For the fabrication of MA-incorporated $PEA_{0.15}(FA_{1-x}MA_x)_{0.85}SnI_3$ compositions, 0.8 M $PEA_{0.15}MA_{0.85}SnI_3$ solution was prepared using MAI (216 mg, 1.36 mmol) instead of FAI. The x = 0.13, 0.25, and 0.50 precursor solutions were prepared by mixing the FA- and MA-based solutions in the ratio of 7:1, 3:1, and 1:1, respectively. The thin films were fabricated in the above-mentioned procedure.

Device fabrication:

Glass/ITO substrates (10 Ω sq^{-1}, Geomatec Co., Ltd.) were etched with zinc powder and HCl (6 M in deionized water), then consecutively cleaned with water, acetone, detergent solution (Semico Clean 56, Furuuchi chemical), water, and isopropyl alcohol with 15 min ultrasonic bath, followed by drying with an air gun. Finally, the organic residues on substrates were removed with plasma treatment. PEDOT:PSS aqueous dispersion was filtered through a 0.45 μm PVDF filter and then spin-coated on the ITO surface at 500 rpm for 10 s and 4000 rpm for 30 s, and then annealed at 140 °C for 20 min under air. The substrates were transferred to an Ar-filled glove box (H_2O, O_2 < 0.1 ppm) and annealed at 140 °C for another 20 min.

The perovskite layer was fabricated on top of PEDOT:PSS following the above-mentioned procedure. Subsequently, 20 mg mL^{-1} solution of **Mono-PC**, **Bis-PC**, **PCBM**, or **ICBA** in chlorobenzene was spin-coated at 2000 rpm for 30 s, followed by annealing at 70 °C for 10 min. 8 nm of bathocuproine (0.01 nm s^{-1}) was then deposited by thermal evaporation. Finally, 100 nm of Ag was deposited through a shadow mask to form the metal electrode. The deposition rate for Ag was set as 0.003 nm s^{-1} until the thickness reached 5 nm, then 0.01 nm s^{-1} until 20 nm, and finally 0.1 nm s^{-1} until the target thickness was reached. The overlap area of the bottom ITO and the uppermost silver electrode of the devices is 0.15 cm^2.

Characterization:

^1H and ^{13}C NMR spectra were recorded with a Bruker Advance III 400 (400 MHz for ^1H and 101 MHz for ^{13}C). Chemical shifts were reported in δ ppm using residual protons in the deuterated solvents for ^1H NMR and using solvent peaks for ^{13}C NMR as internal standards. Mass spectra were measured on timsTOF LC-MS System (IMS-QTOF MS). C_{60} derivatives were purified by a recycling mode of high performance liquid chromatography with the use of a Japan Analytical Industry (JAI) LabACE LC-7080 equipped with a UV detector using COSMOSIL Buckyprep (28 mm ID × 250 mm) and Buckyprep-D (20 mm ID × 250 mm) columns (Nacalai Tesque, Inc.). Column chromatography was performed on silica gel, Merck-Millipore silica gel 60 (0.063-0.2000 mm).

Cyclic voltammetry (CV) was performed on an ALS/chi-620C electrochemical analyzer. The CV cell consisted of a glassy carbon electrode, a Pt wire counter electrode, and an $Ag/AgNO_3$ reference electrode. The measurement was carried out under an argon atmosphere using *o*-dichlorobenzene solutions of samples (1 mM) with 0.1 M tetrabutylammonium hexafluorophosphate ($Bu_4N^+PF_6^-$) as a supporting electrolyte. The redox potentials were calibrated with ferrocene as an internal standard.

Photocurrent–voltage (*J–V*) curves for perovskite solar cells were measured in a nitrogen-filled glovebox (H_2O, O_2 < 1 ppm) with an OTENTO-SUN-P1G solar simulator (BUNKOUKEIKI Co., Ltd.) and a Keithley 2400 SourceMeter. The light intensity of the illumination source was calibrated using a standard silicon photodiode. External quantum efficiency (EQE) were measured by a SMO-250III system equipped with a SM-250 diffuse reflection unit (BUNKOUKEIKI Co., Ltd.). The light intensity of the illumination source was calibrated with a standard SiPD S1337-1010BQ silicon photodiode. The active area of the devices was 0.0985 cm^2 as defined by the aperture of the shadow mask placed between the light source and test cells.

Impedance spectroscopy data was obtained with an E4990A impedance analyser (Keysight) with an oscillator voltage of 30 mV, in the frequency range of 20-200,000 Hz. The measurements were performed with the devices exposed to AM1.5G-equivalent radiation in an inert atmosphere, with a 0.1 cm^2 shadow mask. The impedance data was fit by a series resistor (r_s) along with a capacitor (c_p) in parallel with a resistor (r_p).

X-ray diffraction (XRD) and two-dimensional grazing-incidence X-ray diffraction (2D-GIXD) measurements were performed on Rigaku SmartLab equipped with a hybrid pixel array detector HyPix-3000. Perovskite films were deposited on the surface of PEDOT:PSS with glass/ITO substrates and covered with a thin film of spin-coated poly(methyl methacrylate) (PMMA, Sigma-Aldrich Co.) to prevent direct exposure to air.

Scanning electron microscopy (SEM) was performed with a SU-8010 or SU-8600 (Hitachi High-Technologies Co.) instrument. Atomic force microscopy (AFM) was performed with a Picoscan Plus AFM instrument used in AC-mode with Nanoworld NCST probes. Ellipsometry measurement was conducted by Stokes ellipsometer LSE-100 (Gaertner Scientific). Photoelectron yield spectroscopy (PYS) measurements were carried out using a BUNKOUKEIKI BIP-KV201 (accuracy: ± 0.02 eV, extraction voltage = 10 V) under vacuum (< 10^{-2} Pa). Perovskite film samples for PYS measurements were prepared by deposition of the precursor solution on the surface of PEDOT:PSS with ITO as substrates in an Ar-filled glove box and transferred to the chamber for PYS measurement without exposure to air.

Details of the Low-energy inverse photoelectron spectroscopy (LEIPS) apparatus are given elsewhere.[4] An electron beam is incident to the sample surface, and the emitted photons are detected using a bandpass filter and a photomultiplier. To reduce systematic error, the LEIPS measurements were performed at two wavelengths (260 and 285 nm) to determine electron affinity (EA). The vacuum level (E_{VL}) was determined from the inflection point of low-energy electron transmission (LEET), *i.e.*, the sample current as a function of the electron energy. EA was determined as the onset energy of the LEIPS spectrum with respect to E_{VL}. The thickness dependence of EA at thicknesses t = 5, 10, and 15 nm was investigated to ensure that the measured values are not affected by the sample charging or the substrate. Errors were estimated statistically from EAs measured for the different wavelengths and samples (Figure S5).

For the time-resolved photoluminescence (TRPL) measurements, the samples were excited by a picosecond pulsed light with a wavelength of 688 nm (Advanced Laser Diode System). The excitation fluence was set at 100 nJ cm^{-2}. The PL signals were recorded using an avalanche photodiode (ID Quantique) and a time-correlated single photon counting board (PicoQuant). The PL lifetimes were obtained by fitting the PL decay curve with an exponential function. The PL spectra were recorded using an InGaAs array detector equipped with a monochromator (Princeton Instruments). The samples were kept in an Ar-filled metallic box for the whole process to avoid oxygen contamination and degradation.

Synthesis of Mono-PC.

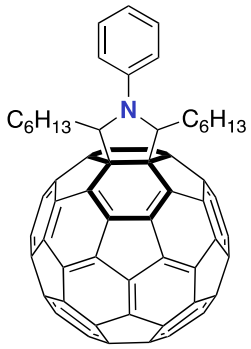

A chlorobenzene solution (150 mL) of heptanal (2.0 mL), 2-(phenylamino)octanoic acid (118 mg, 0.50 mmol), and C_{60} (360 mg, 0.50 mmol) was stirred under N_2 atmosphere at 120 °C for 24 h and concentrated under reduced pressure. The crude product was purified by preparative recycling HPLC (Buckyprep, toluene) to give **Mono-PC** (113 mg, 22.4%) as blown powder. ^{1}H NMR (400 MHz, $CDCl_3/CS_2$ = 1/1, v/v): δ 0.87 (t, J = 6.4 Hz, 6H), 1.21–1.38 (m, 12H), 1.48–1.69 (m, 4H), 2.26–2.36 (m, 2H), 2.46–2.58 (m, 2H), 5.13 (t, J = 6.4 Hz, 2H), 7.17–7.20 (m, 1H), 7.44–7.50 (m, 4H); ^{13}C NMR (101 MHz, $CDCl_3/CS_2$ = 1/1, v/v): δ 14.4, 23.0, 28.3, 30.0, 31.9, 34.6, 74.0, 74.7, 122.0, 123.4, 125.3, 129.2, 129.7, 135.3, 137.6, 139.7, 140.0, 141.7, 141.8, 142.2, 142.4, 142.8, 143.2, 143.3, 144.5, 144.7, 145.2, 145.3, 145.4, 145.8, 146.1, 146.2, 146.4, 146.6, 147.1, 147.3, 153.3, 155.5; HRMS (APCI) (*m/z*) $[M+H]^+$ calcd. For $C_{80}H_{34}N$, 1008.2686; found, 1008.2687.

Synthesis of Bis-PC

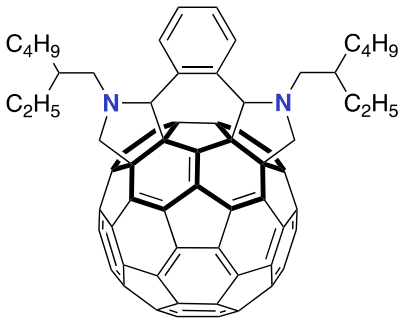

A *o*-dichlorobenzene solution (150 mL) of *o*-phthalaldehyde (155mg, 1.15 mmol), *N*-(2-ethylhexyl)glycine (570 mg, 3.20 mmol), and [60]fullerene (720 mg, 1.00 mmol) was stirred under N_2 atmosphere at 120 °C for 18 h and concentrated under reduced pressure. The crude product was purified by column chromatography (SiO_2, *n*-hexane:toluene, 100:1-10:1) and by preparative recycling HPLC (Buckyprep-D, toluene) to give **Bis-PC** (243 mg, 22.0%) as brown powder. ^{1}H NMR (400 MHz, $CDCl_3/CS_2$ = 1/1, v/v): δ 0.96-1.14 (m, 12H), 1.29–1.65 (m, 14H), 1.86-1.95 (m, 2H), 2.06–2.21 (m, 2H), 2.43–2.47 (m, 2H), 3.36 (t, J = 7.6 Hz, 2H), 3.73 (d, J =

10.0 Hz, 2H), 4.70 (s, 2H), 4.73 (d, J = 10.0 Hz, 2H), 7.35–7.37 (m, 2H), 7.88–7.91 (m, 2H); ^{13}C NMR (101 MHz, $CDCl_3/CS_2$ = 1/1, v/v): δ 11.6, 14.5, 14.7, 23.6, 23.7, 24.7, 25.7, 29.3, 29.5, 31.2, 32.2, 39.0, 39.0, 60.6, 60.7, 63.2, 63.2, 67.0, 67.1, 68.6, 68.7, 77.5, 80.0, 80.0, 122.8, 125.5, 127.4, 127.7, 127.7, 128.4, 129.1, 133.7, 133.7, 133.9, 138.2, 138.2, 138.3, 138.6, 140.8, 142.0, 143.5, 143.9, 144.2, 144.4, 145.1, 145.2, 145.5, 145.5, 145.6, 146.0, 146.2, 146.2, 146.3, 146.3, 146.4, 146.7, 147.7, 147.7, 148.4, 148.8, 148.9, 149.4, 150.2, 155.8, 158.6; HRMS (APCI) (*m/z*) $[M+H]^+$ calcd. For $C_{86}H_{45}N_2$, 1105.3577; found, 1105.3570.

X-ray Crystal Structure Analysis:

Single crystals of **Bis-PC** suitable for X-ray structural analysis were obtained by slowly cooling the solution of **Bis-PC** in chlorobenzene. Diffraction data was collected at 100 K on a Rigaku Oxford Diffraction XtaLAB Synergy-R with Mo Kα radiation (λ = 0.71073 Å) and equipped with a hybrid pixel array detector HyPix-6000HE. A total of 34635 reflections were measured with a maximum 2θ angle of 52.7˚, of which 10457 were independent reflections (R_{int} = 0.1011). The structure was solved by direct methods (SHELXS-2018/3[5]) and refined by the full-matrix least-squares on F^2 (SHELXL-2018/3). All non-hydrogen atoms were refined anisotropically. All hydrogen atoms were placed using AFIX instructions. The crystal data are as follows: $C_{14}H_{30}N_2Si_2$; FW = 282.57, crystal size 0.20 × 0.21 × 0.22 mm, Triclinic, P-1, a = 15.8224(5) Å, b = 21.9763(6) Å, c = 28.7119(12) Å, β = 93.501(3)°, V = 9965.0(6) Å^3, Z = 8, D_c = 1.473 g cm^{-3}. The refinement converged to R_1 = 0.1094 ($I > 2\sigma(I)$), wR_2 = 0.2343 (all data), GOF = 1.134.

Crystallographic data have been deposited with the Cambridge Crystallographic Data Center as supplementary publication no. CCDC-2369060. These data can be obtained free of charge from The Cambridge Crystallographic Data Centre via www.ccdc.cam.ac.uk/data_request/cif.

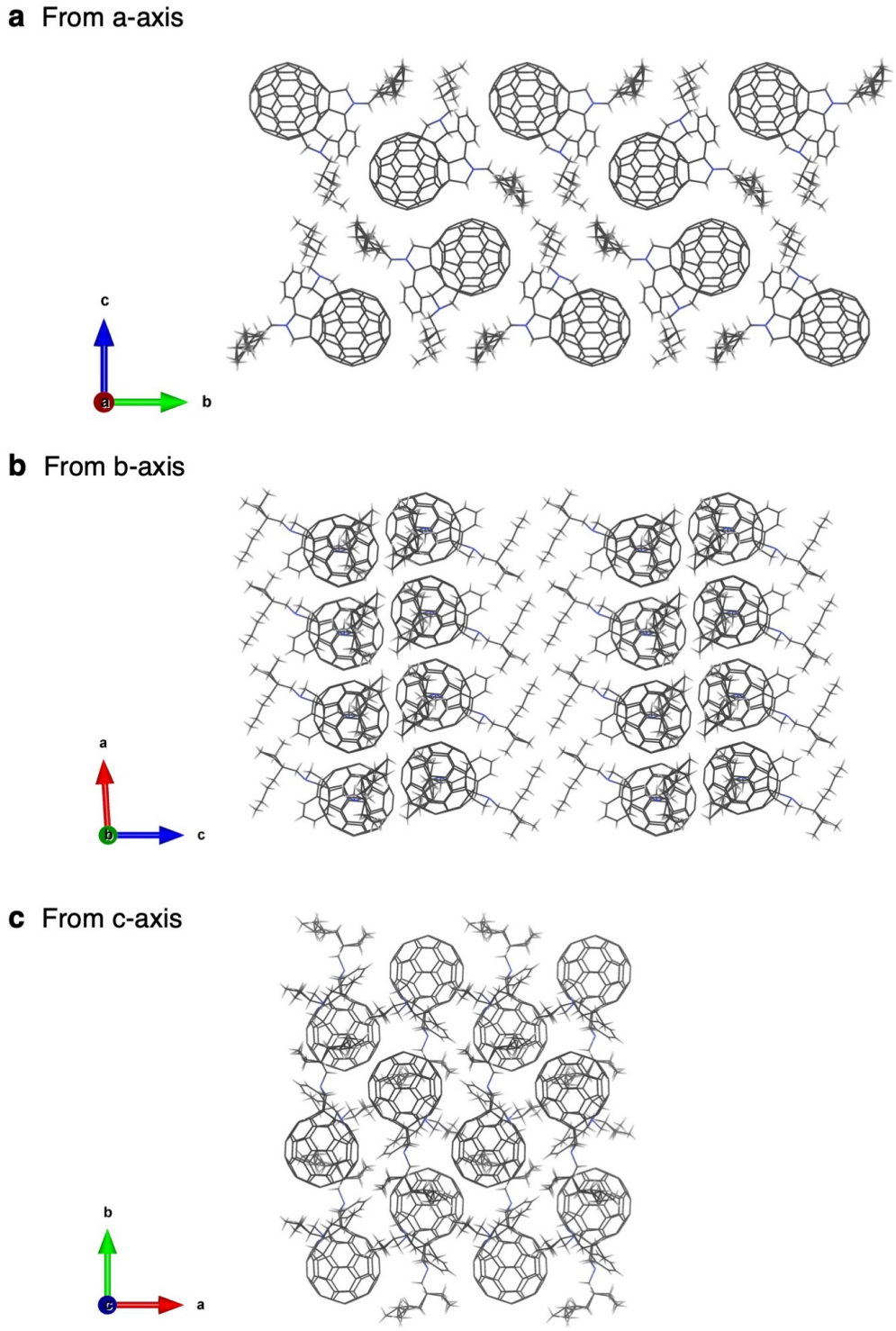

Figure S1. Packing structure of **Bis-PC**, viewed from (a) a-axis, (b) b-axis, and (c) c-axis.

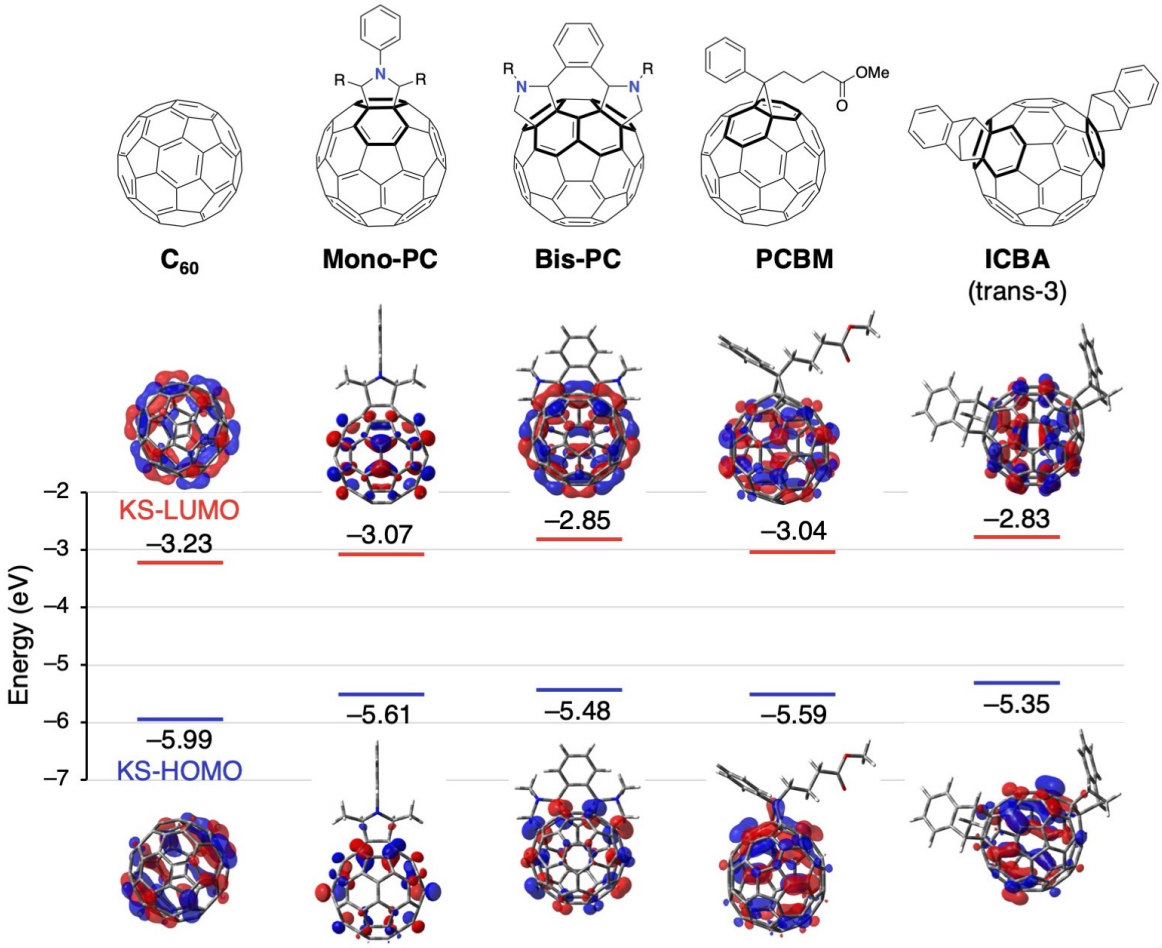

Figure S2. Calculated Kohn–Sham (KS)-HOMO and LUMO energy levels and depictions of frontier orbitals (isovalue: 0.03) for fullerene derivatives. Optimized structures were calculated at the B3LYP/6-31G(d) level of theory.

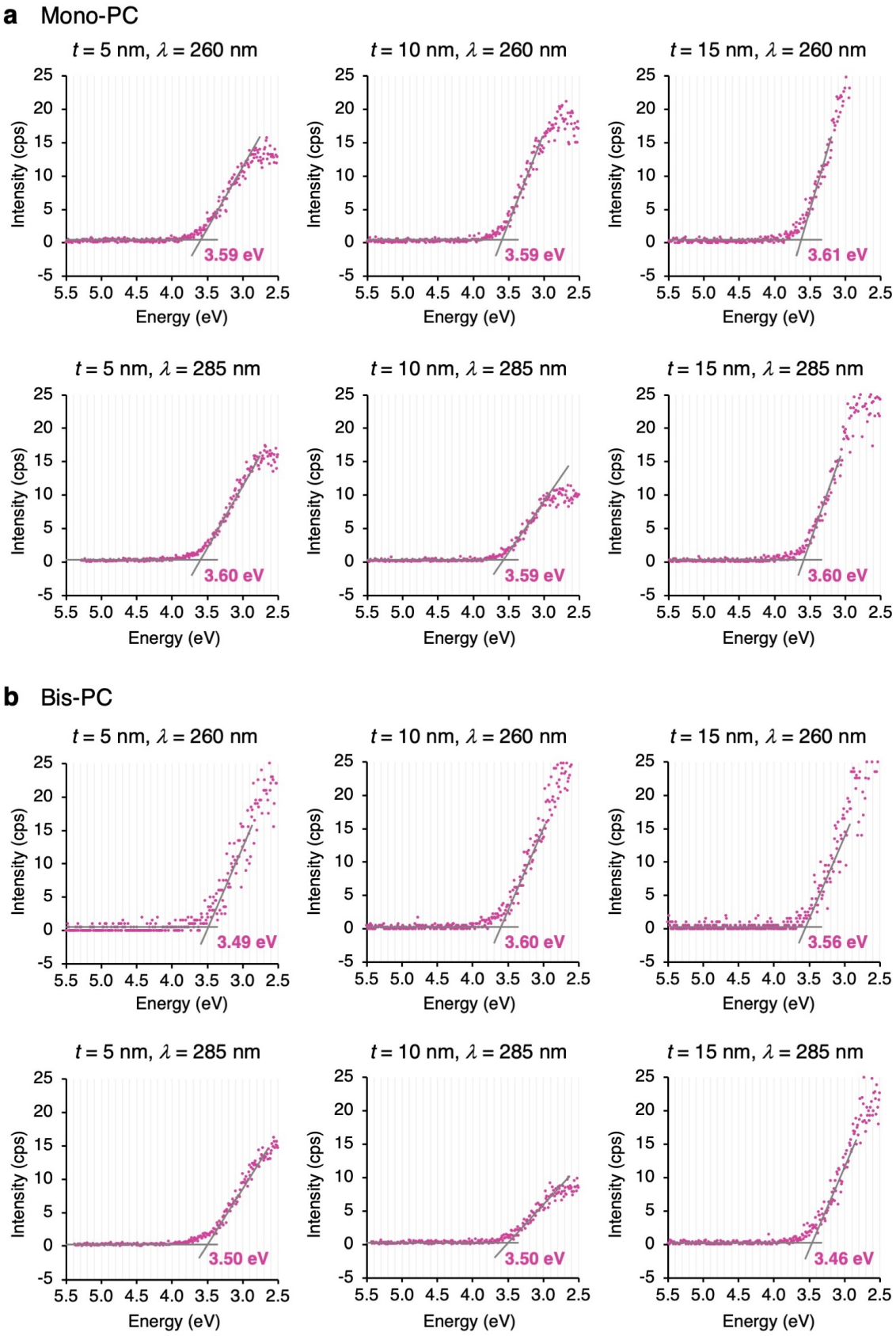

Figure S3. Low-energy inverse photoelectron spectroscopy (LEIPS) spectra of (a) **Mono-PC** and (b) **Bis-PC**, conducted for 5, 10, and 15 nm-thick films at two wavelengths of bandpass filter (260 and 285 nm).

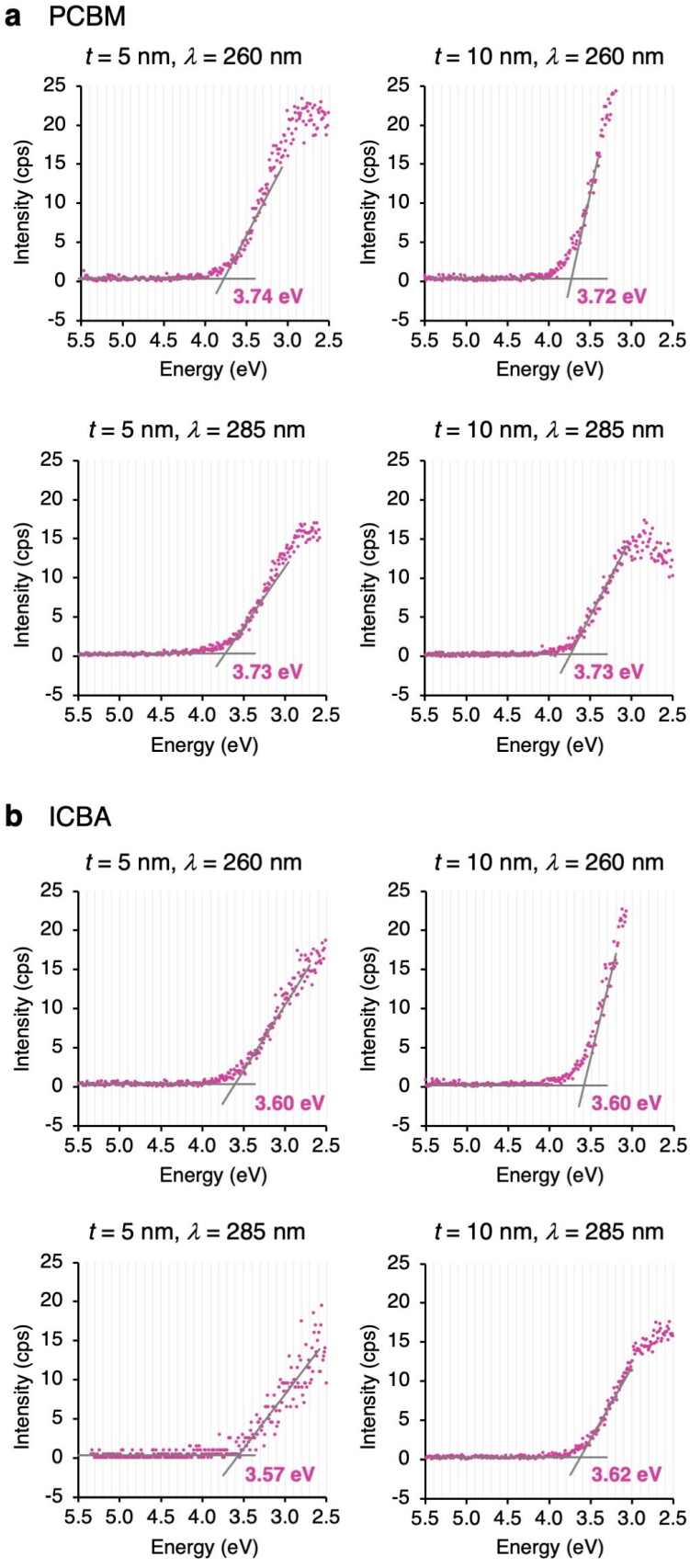

Figure S4. LEIPS spectra of (a) **PCBM** and (b) **ICBA**, conducted for 5 and 10 nm-thick films with two wavelengths of bandpass filter (260 and 285 nm).

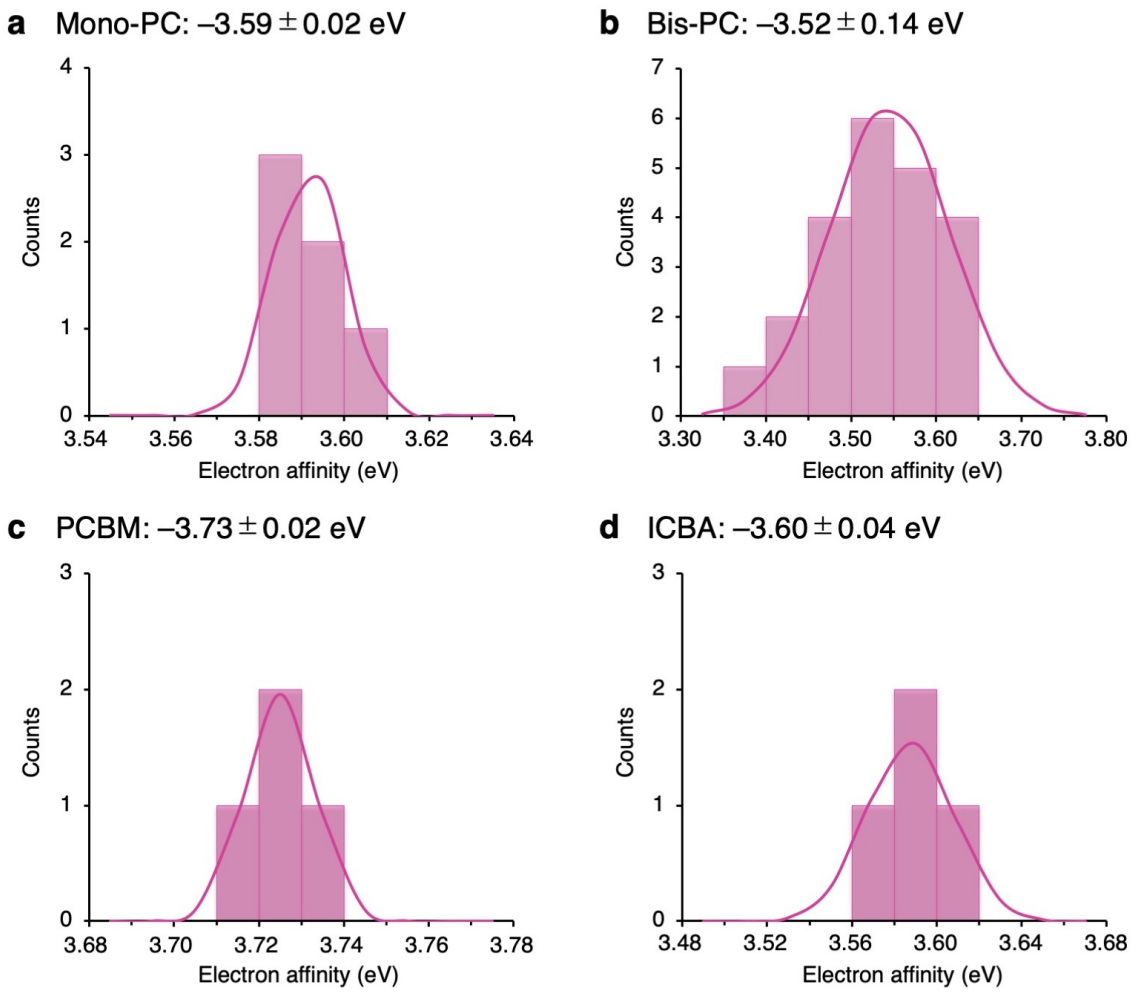

Figure S5. Distributions of the measured electron affinities (EAs) for (a) **Mono-PC**, (b) **Bis-PC**, (c) **PCBM** and (d) **ICBA**.

Table S1. Film thickness of fullerene derivatives estimated by ellipsometry.

	Mono-PC	**Bis-PC**	**PCBM**	**ICBA**
	47.1	49.7	45.2	48.1
	47.0	49.8	45.2	48.0
	47.2	49.6	45.3	48.2
	47.4	49.4	45.2	48.3
Average	47.2±0.1	49.6±0.1	45.2±0.0	48.2±0.1

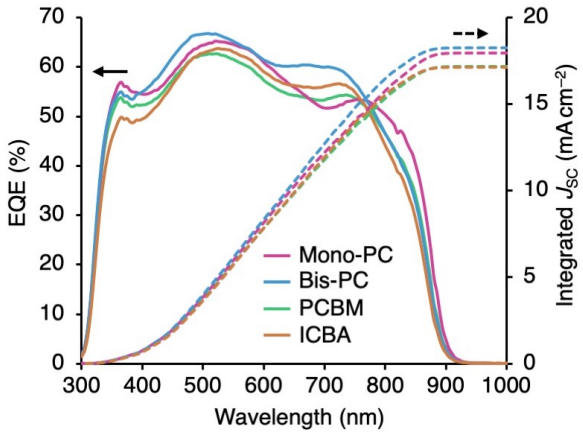

Figure S6. Incident photon-to-electron conversion efficiency (IPCE) spectra of tin perovskite solar cells using different electron-transporting materials.

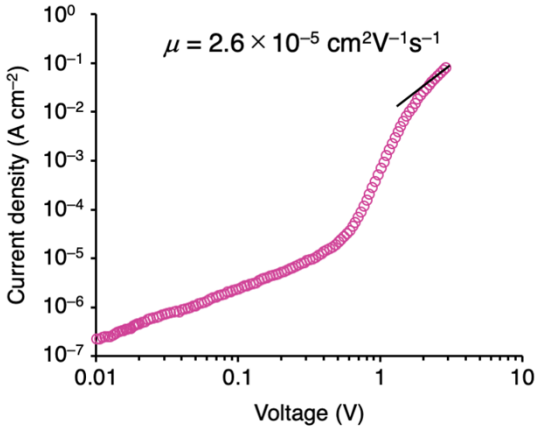

Figure S7. Space-charge-limited current (SCLC) *J*–*V* characteristics obtained in the dark for electron-only ITO/SnO_2/**Bis-PC**/BCP/Ag devices. Electron mobilities were estimated using the Mott-Gurney law: $J = (9/8)\varepsilon\varepsilon_0\mu(V^2/d^3)$, where J is the current density, ε_0 is the permittivity of free space (8.85×10^{-12} F m^{-1}), ε is the relative permittivity of the material (3.9 for fullerenes),[6] μ is the electron mobility, V is the applied voltage, and d is the thickness of the active layer (49.6 nm), respectively. The estimated electron mobility was 2.6×10^{-5} cm^{2}V^{-1}s^{-1}, which is lower than that of **ICBA** (4.5×10^{-5} cm^{2}V^{-1}s^{-1}).[7]

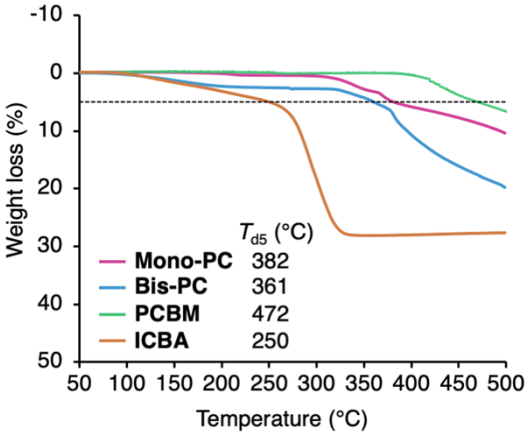

Figure S8. Thermogravimetric analysis (TGA) of fullerene derivatives under a nitrogen atmosphere with a rate of 5 °C min^{-1}. The decomposition temperature estimated by 5% weight loss, T_{d5}, was 382, 361, 472, and 250 °C for **Mono-PC**, **Bis-PC**, **PCBM**, and **ICBA**, respectively.

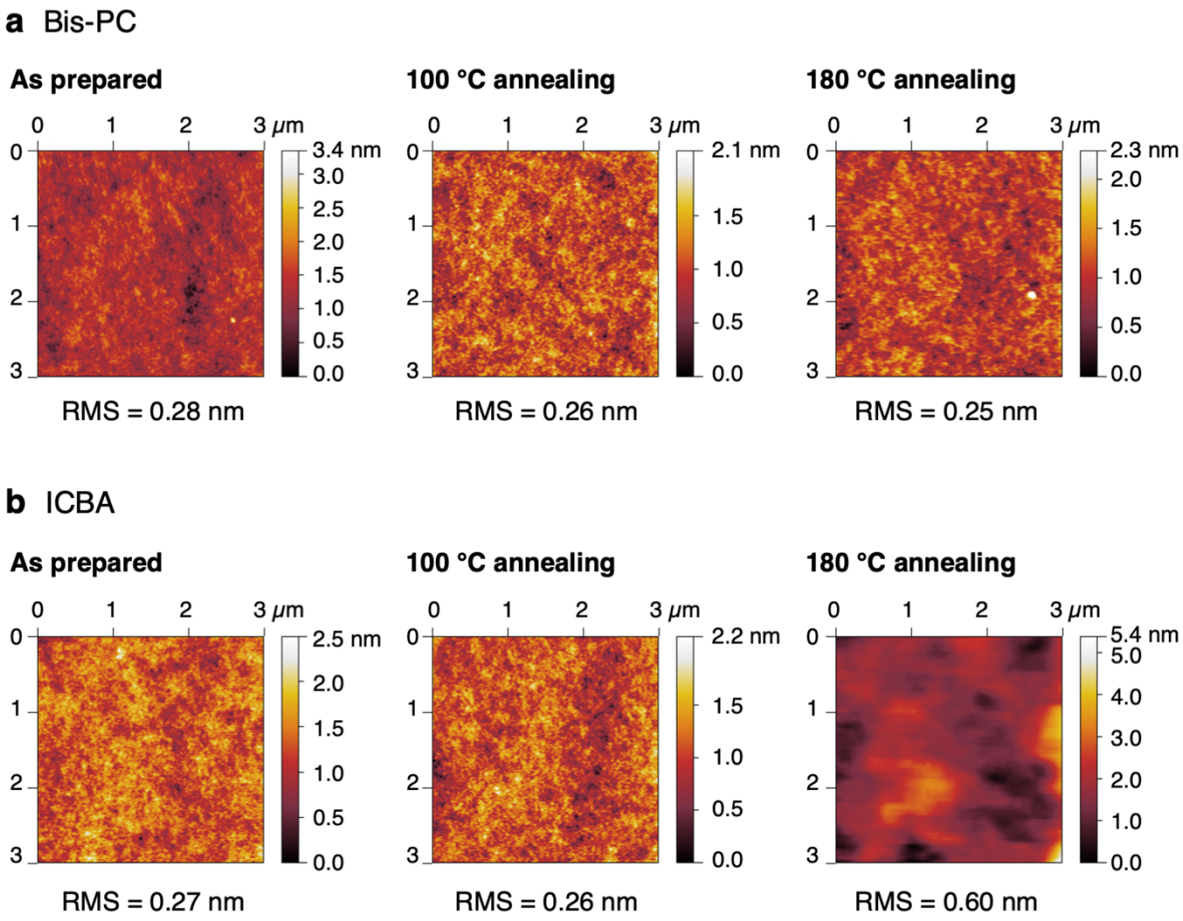

Figure S9. The film thermal test. AFM images of (a) **Bis-PC** and (b) **ICBA** thin films on glass substrates as prepared, annealed at 100 °C for 30 min, and annealed at 180 °C for 30 min. The root-mean-square (RMS) roughness is also shown. By annealing the thin films at 180 °C, a change in the morphology of **ICBA** films was observed with increased RMS roughness from 0.27 nm to 0.60 nm, whereas the morphology of **Bis-PC** film remains unchanged.

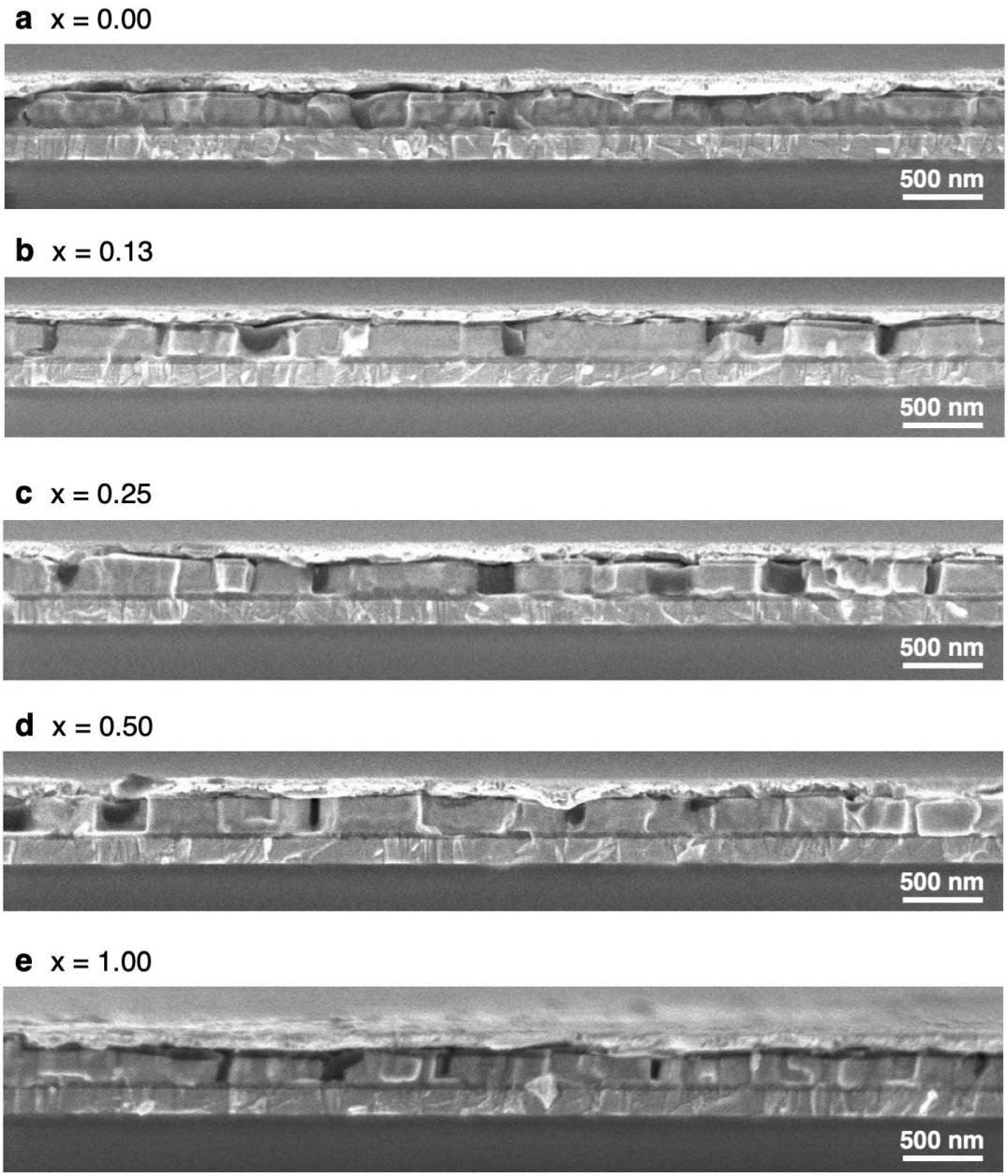

Figure S10. Cross-sectional scanning electron microscopy (SEM) images of solar cells using perovskite composition of $PEA_{0.15}(FA_{1-x}MA_x)_{0.85}SnI_3$ (x = 0.00, 0.13, 0.25, 0.50, 1.00) with **Bis-PC** as electron-transporting material.

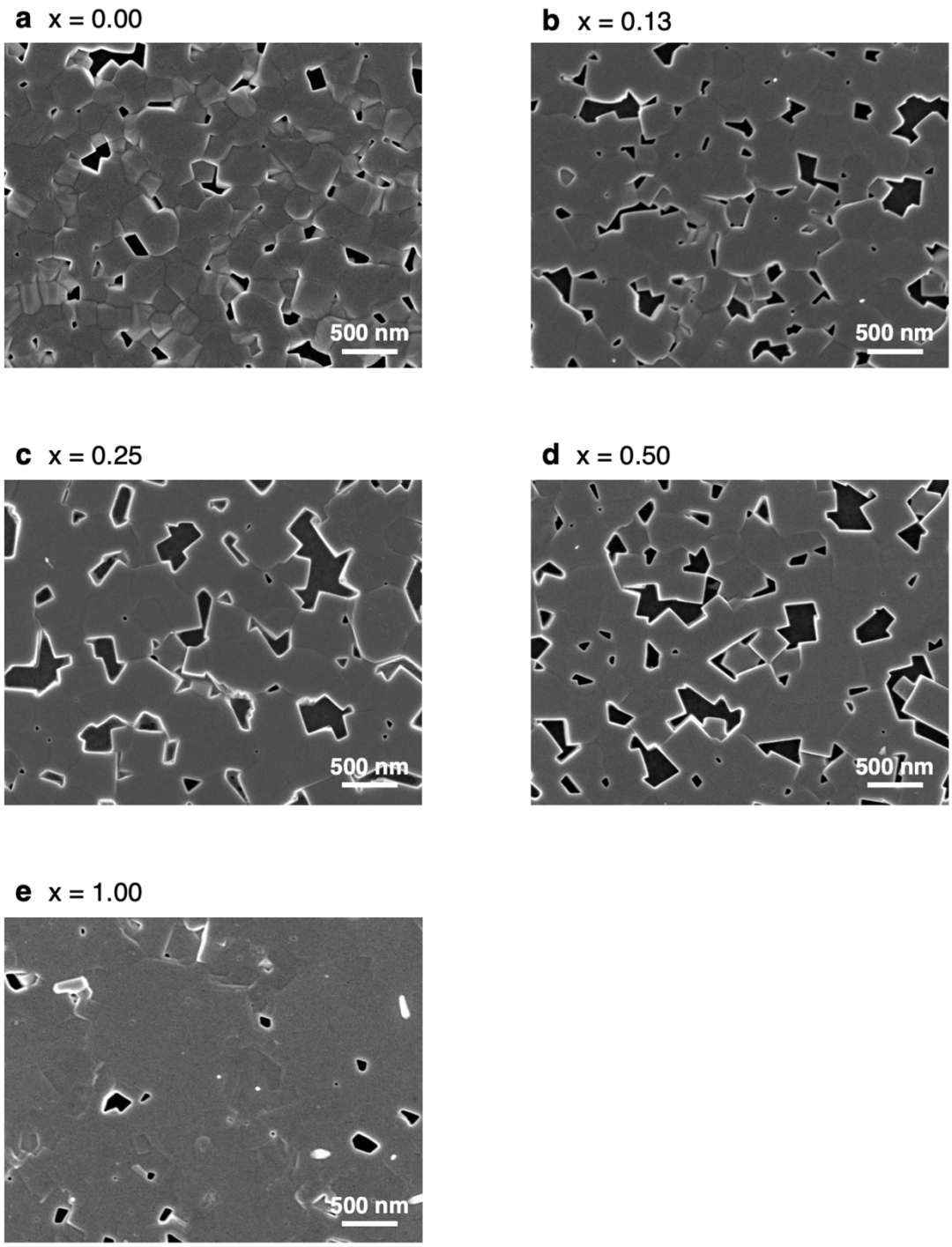

Figure S11. Surface SEM images of perovskite films with the composition of $PEA_{0.15}(FA_{1-x}MA_x)_{0.85}SnI_3$ (x = 0.00, 0.13, 0.25, 0.50, 1.00).

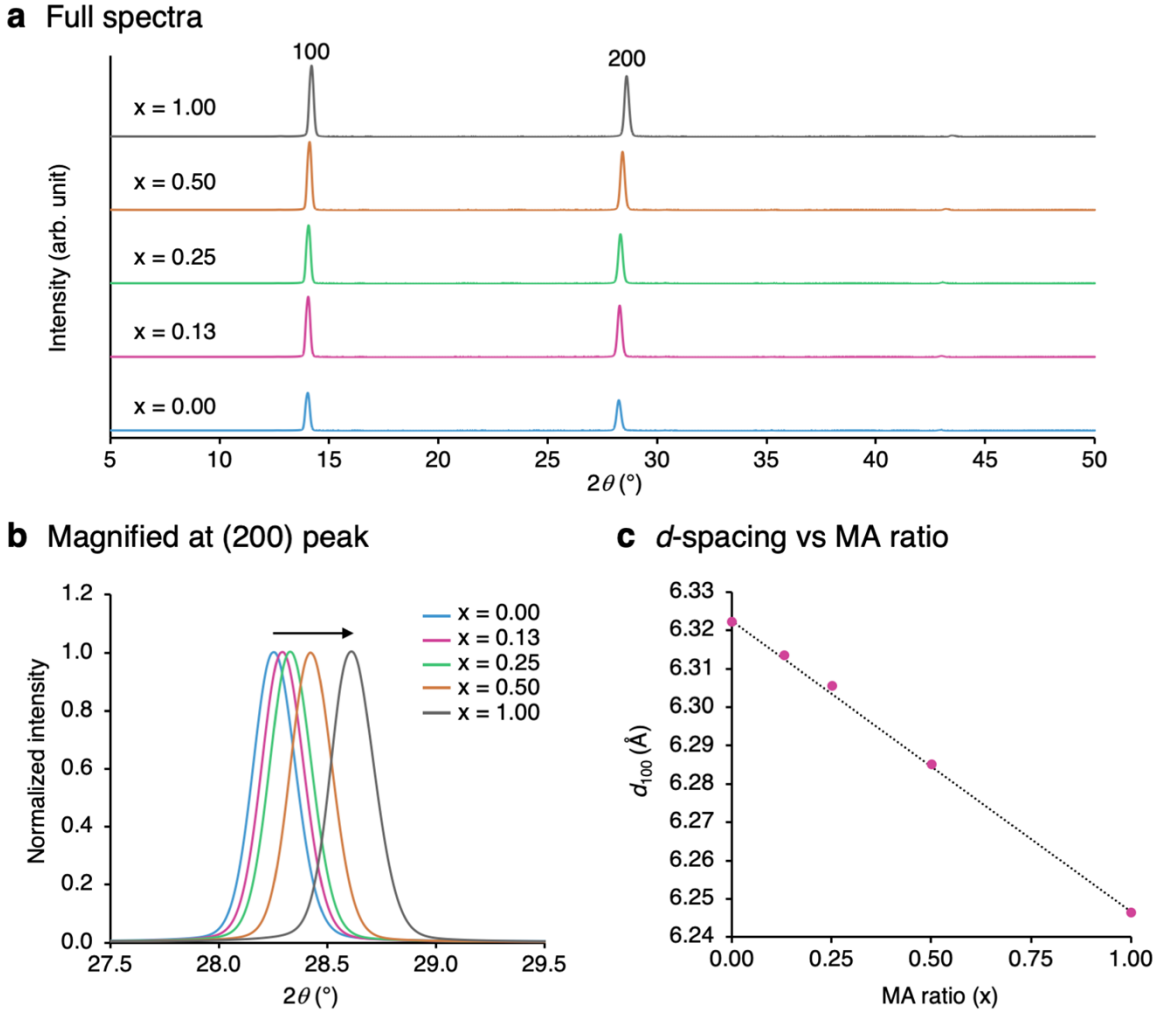

Figure S12. (a) Full and (b) magnified X-ray diffraction (XRD) spectra of $PEA_{0.15}(FA_{1-x}MA_x)_{0.85}SnI_3$ (x = 0.00, 0.13, 0.25, 0.50, 1.00) films. (c) Plot of the interplanar spacing (d_{100}) against the MA ratio (x).

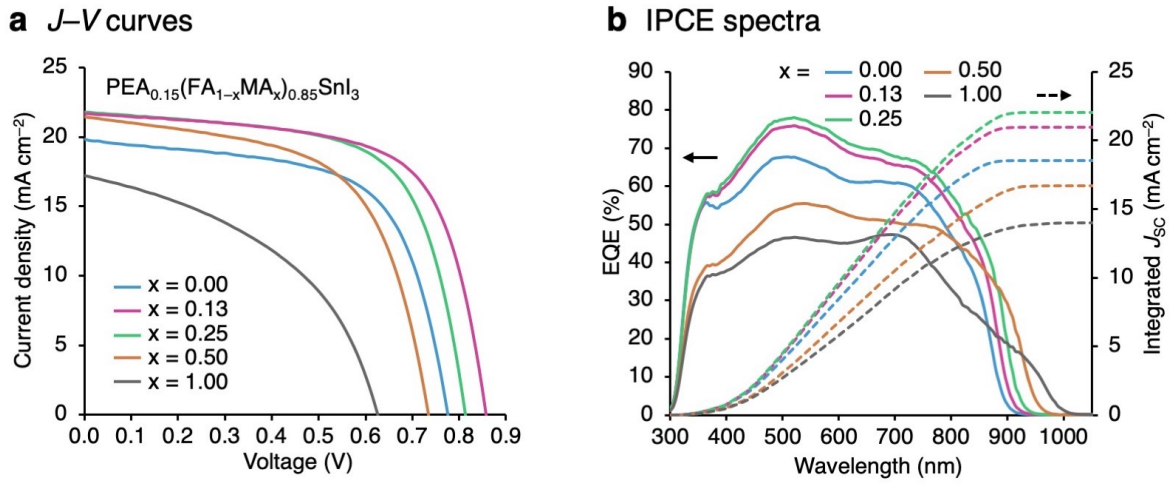

Figure S13. (a) *J–V* curves and (b) IPCE spectra of tin perovskite solar cells using perovskite composition of $PEA_{0.15}(FA_{1-x}MA_x)_{0.85}SnI_3$ (x = 0.00, 0.13, 0.25, 0.50, 1.00) with **Bis-PC** as electron-transporting material.

Table S2. Photovoltaic parameters of tin perovskite solar cells using $PEA_{0.15}(FA_{1-x}MA_x)_{0.85}SnI_3$ (x = 0.00, 0.13, 0.25, 0.50, 1.00) perovskite composition.

x	J_{SC} (mA cm^{-2}) [a]	V_{OC} (V) [a]	FF [a]	PCE (%) [a]
0.00	19.85 (19.7±0.6)	0.78 (0.74±0.02)	0.63 (0.63±0.01)	9.70 (9.2±0.7)
0.13	21.69 (20.7±0.6)	0.86 (0.81±0.02)	0.66 (0.66±0.01)	12.27 (11.2±0.4)
0.25	21.79 (20.2±1.5)	0.81 (0.80±0.02)	0.65 (0.64±0.01)	11.57 (10.3±0.8)
0.50	21.44 (18.3±2.4)	0.73 (0.71±0.02)	0.59 (0.56±0.04)	9.35 (7.4±1.4)
1.00	17.22 (16.1±0.7)	0.63 (0.61±0.01)	0.44 (0.42±0.02)	4.77 (4.2±0.4)

[a] The average and standard deviation values for 12 devices were given in parentheses.

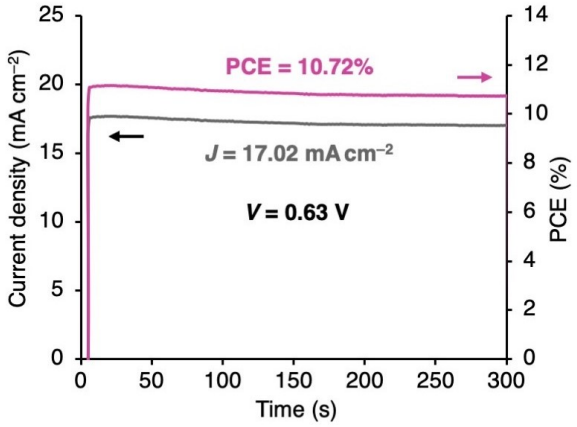

Figure S14. Stabilized current density (black line) and stabilized power output (red line) of a representative **Bis-PC**-based perovskite solar cell with $PEA_{0.15}(FA_{0.87}MA_{0.13})_{0.85}SnI_3$ composition, measured at a bias of 0.63 V under AM 1.5G, 100 mW cm^{-2} irradiation.

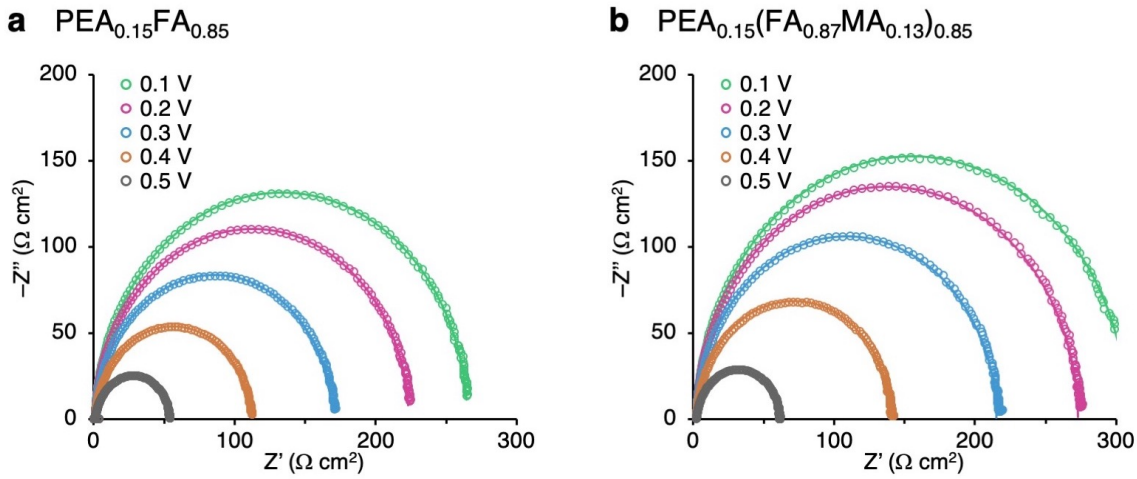

Figure S15. Electrical impedance spectra for (a) $PEA_{0.15}FA_{0.85}SnI_3$ (x = 0.00) and (b) $PEA_{0.15}(FA_{0.87}MA_{0.13})_{0.85}SnI_3$ (x = 0.13) solar cells at a bias voltage of 0.1–0.5 V under AM 1.5G, 100 mW cm^{-2} irradiation.

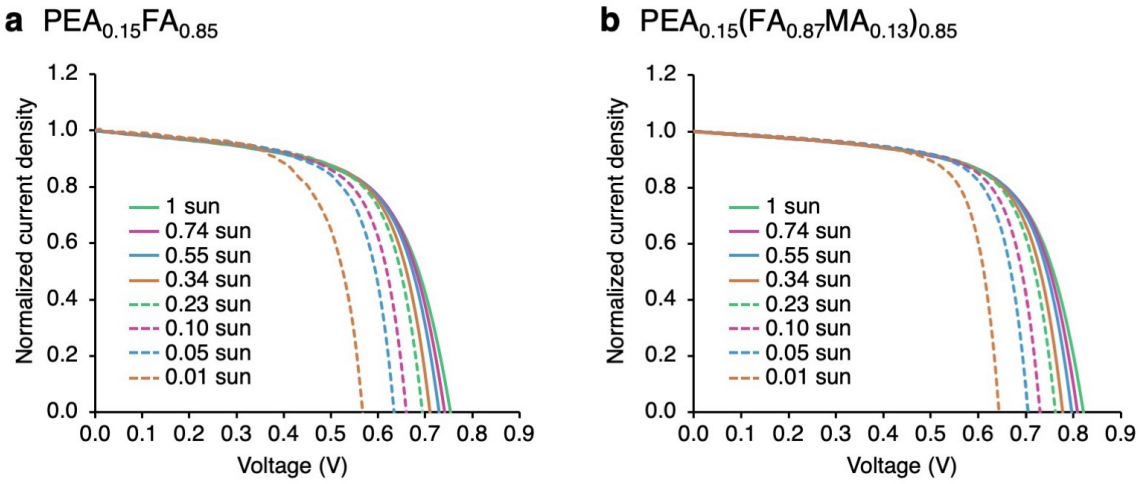

Figure S16. *J–V* curves of (a) $PEA_{0.15}FA_{0.85}SnI_3$ (x = 0.00) and (b) $PEA_{0.15}(FA_{0.87}MA_{0.13})_{0.85}SnI_3$ (x = 0.13) solar cells with different light intensity (1–0.01 sun).

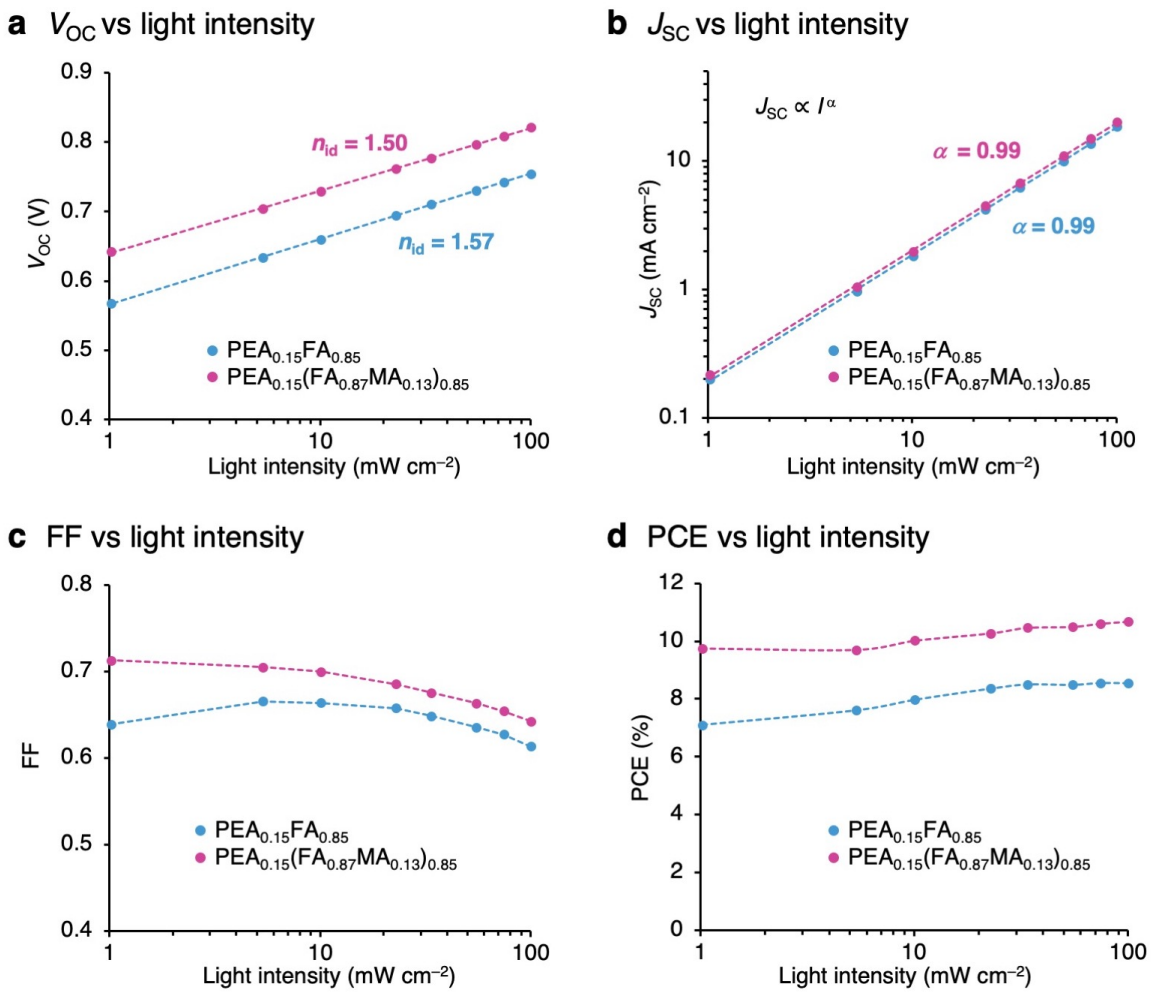

Figure S17. Light intensity dependence of (a) open-circuit voltage (V_{OC}), (b) current density (J_{SC}), (c) fill factor (FF), and (d) power conversion efficiency (PCE).

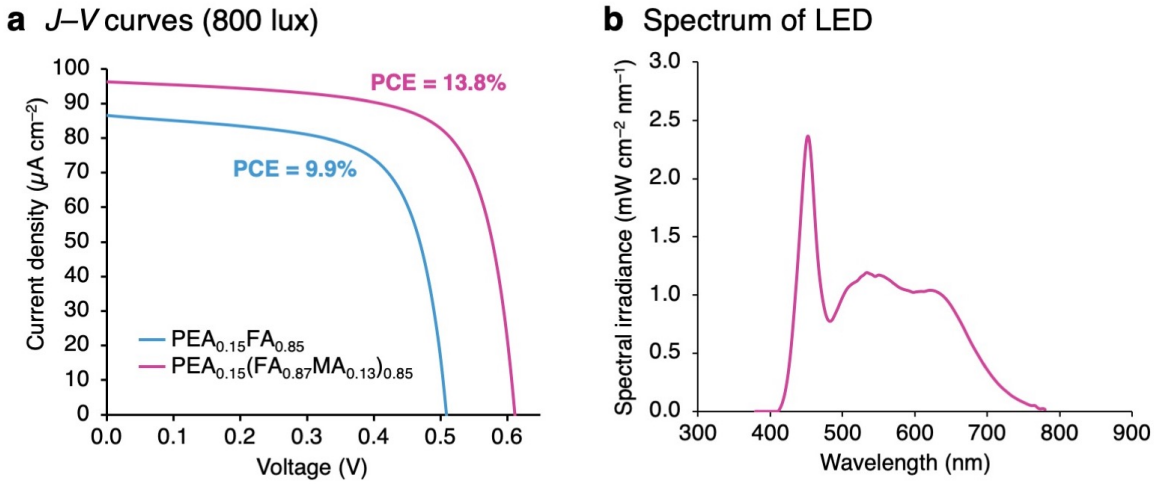

Figure S18. (a) *J–V* curves under the low light intensity of 800 lux using white LED. (b) Spectrum of white LED.

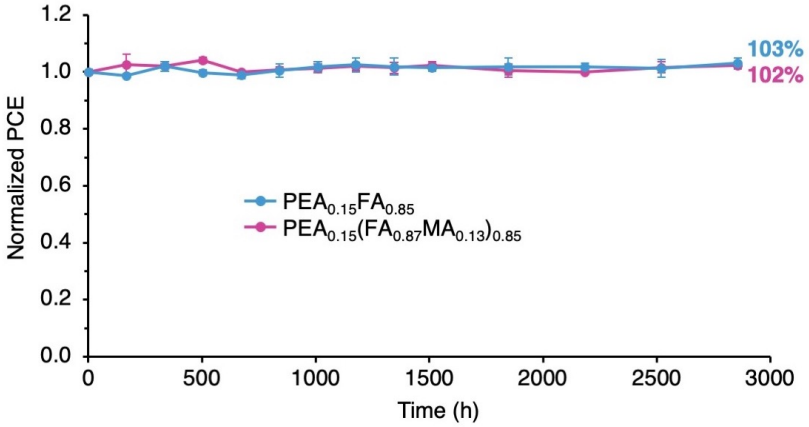

Figure S19. Long-term stability of **Bis-PC**-based perovskite solar cells for $PEA_{0.15}FA_{0.85}SnI_3$ (x = 0.00) and $PEA_{0.15}(FA_{0.87}MA_{0.13})_{0.85}SnI_3$ (x = 0.13) compositions under nitrogen atmosphere.

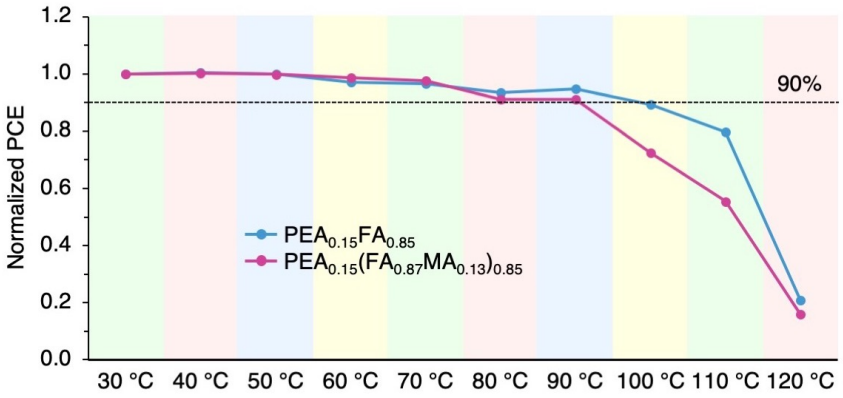

Figure S20. Thermostability of **Bis-PC**-based perovskite solar cells for $PEA_{0.15}FA_{0.85}SnI_3$ (x = 0.00) and $PEA_{0.15}(FA_{0.87}MA_{0.13})_{0.85}SnI_3$ (x = 0.13) compositions. The solar cell device was heated at the specified temperature for 1 h, and then the performance was evaluated by *J–V* measurement. This measurement set was repeated with raising the temperature by 10 °C.

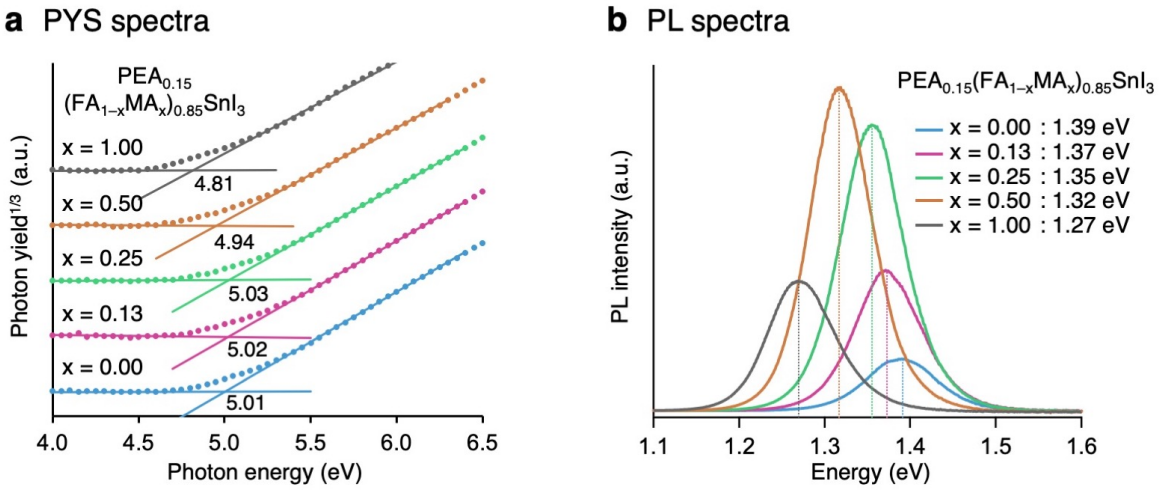

Figure S21. (a) Photoemission yield spectroscopy (PYS) and (b) photoluminescence (PL) spectra of $PEA_{0.15}(FA_{1-x}MA_x)_{0.85}SnI_3$ films (x = 0.00, 0.13, 0.25, 0.50, 1.00) fabricated on glass/ITO/PEDOT:PSS substrates.

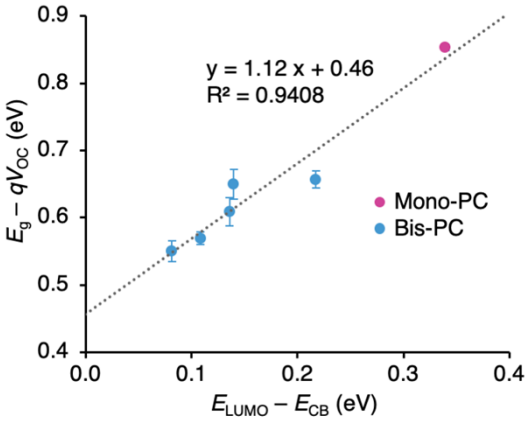

Figure S22. Plot showing the relationship between energy offset ($E_{LUMO} - E_{CB}$) and voltage loss ($E_g - qV_{OC}$).

NMR and HRMS spectra:

^{1}H NMR spectrum (400 MHz, $CDCl_3/CS_2$ = 1/1) of **Mono-PC**

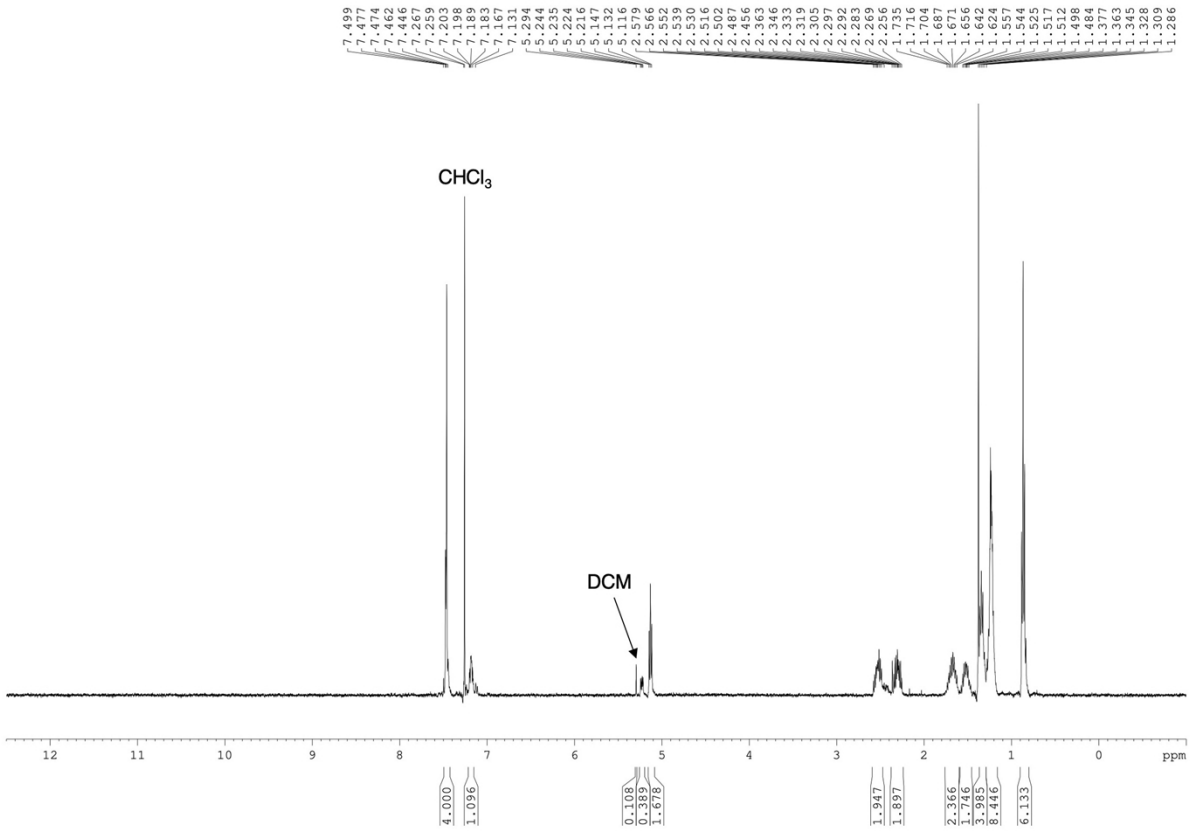

^{13}C NMR spectrum (101 MHz, $CDCl_3/CS_2$ = 1/1) of **Mono-PC**

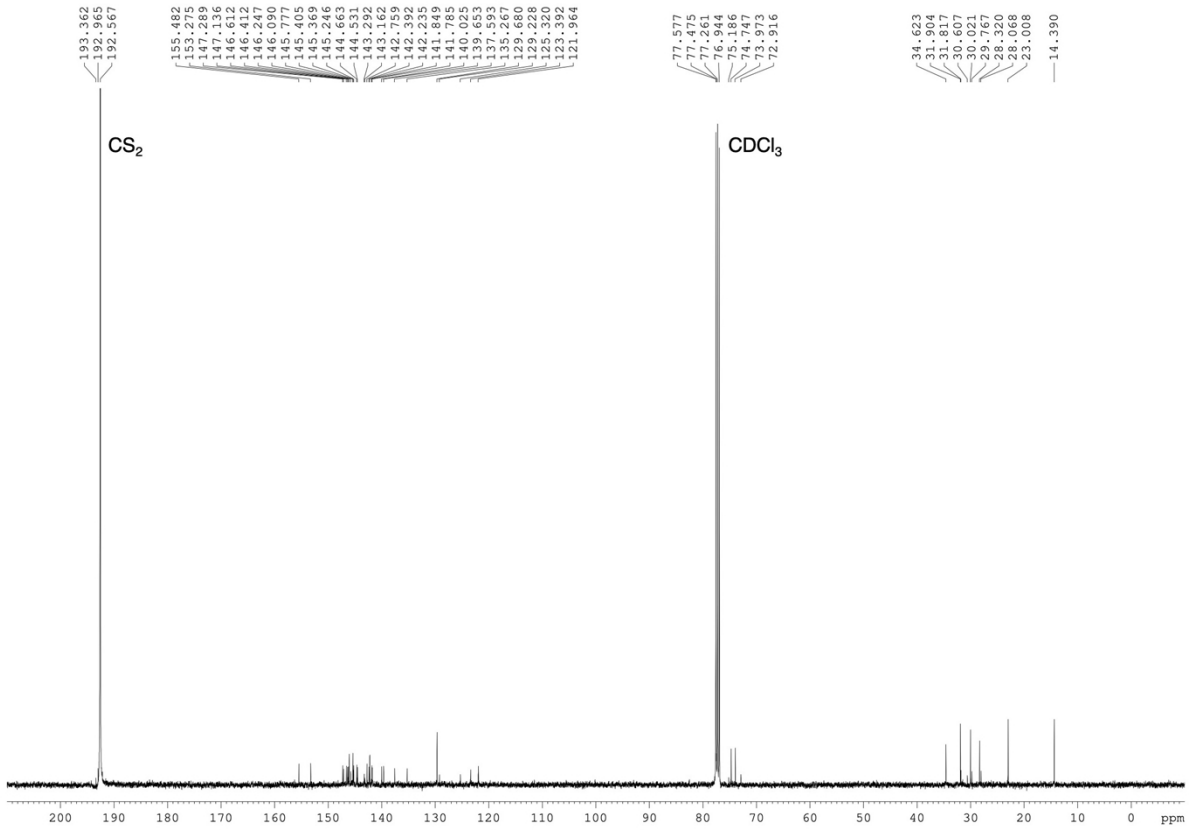

HRMS spectrum (APCI) of **Mono-PC**

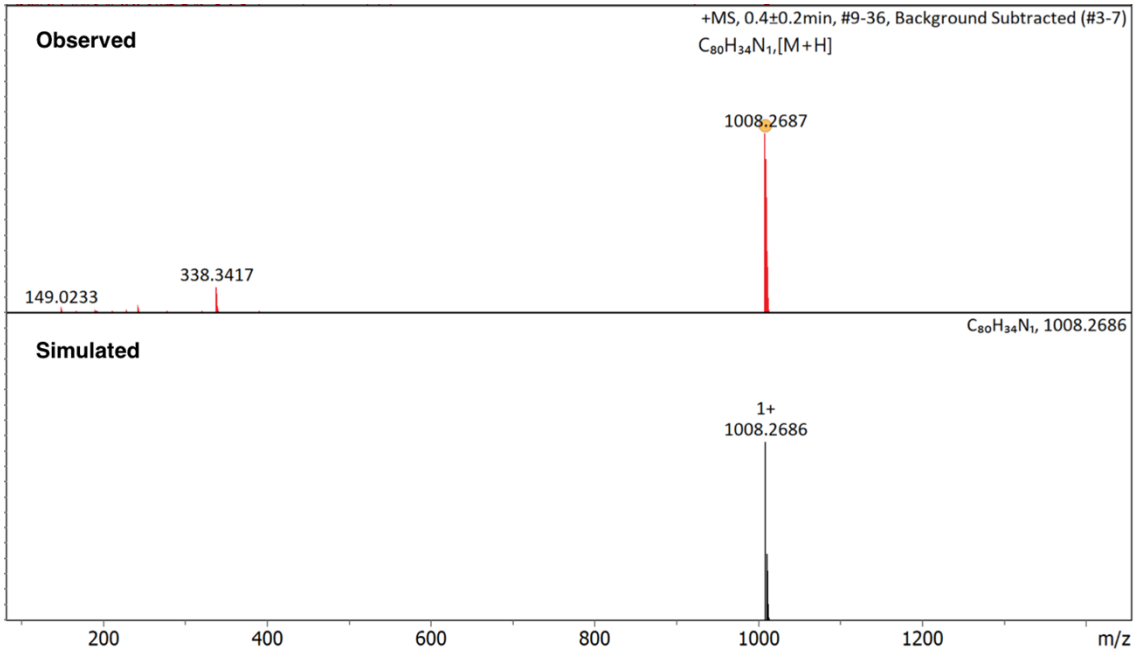

^{1}H NMR spectrum (400 MHz, $CDCl_3/CS_2$ = 1/1) of **Bis-PC**

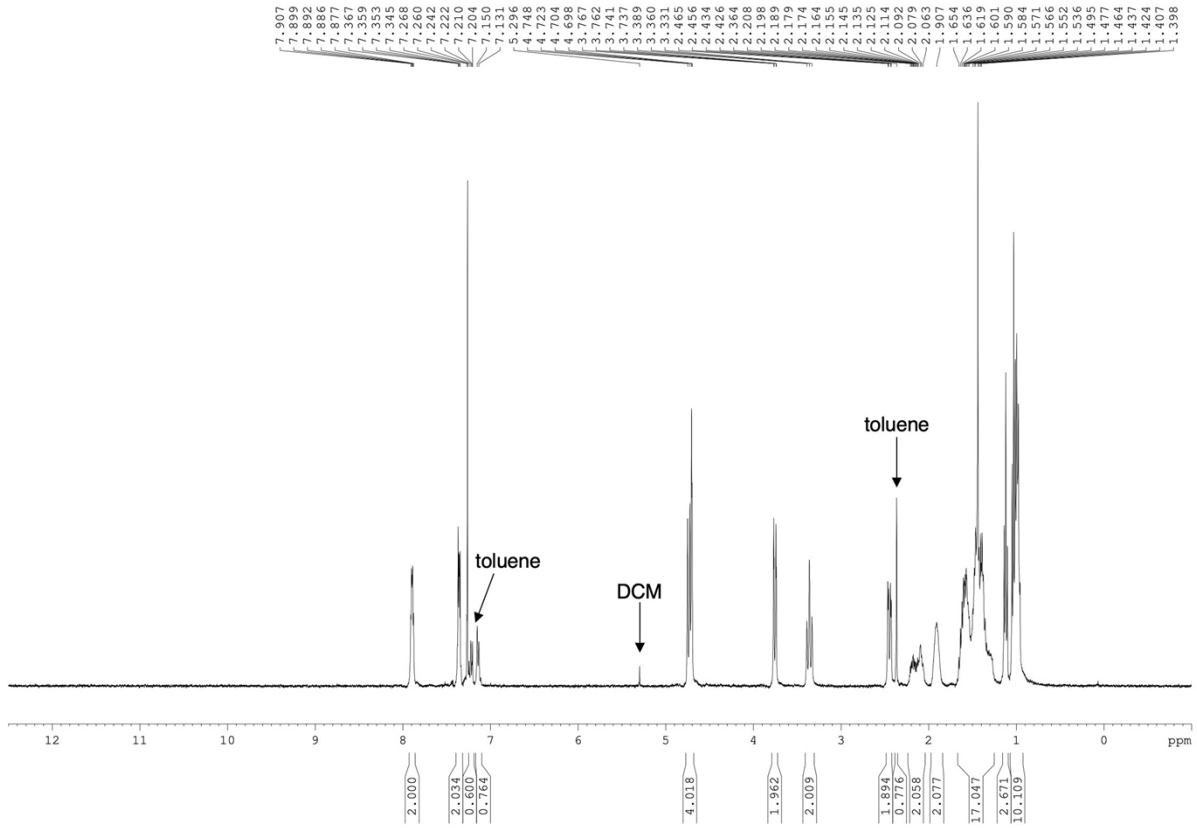

^{13}C NMR spectrum (101 MHz, $CDCl_3/CS_2$ = 1/1) of **Bis-PC**

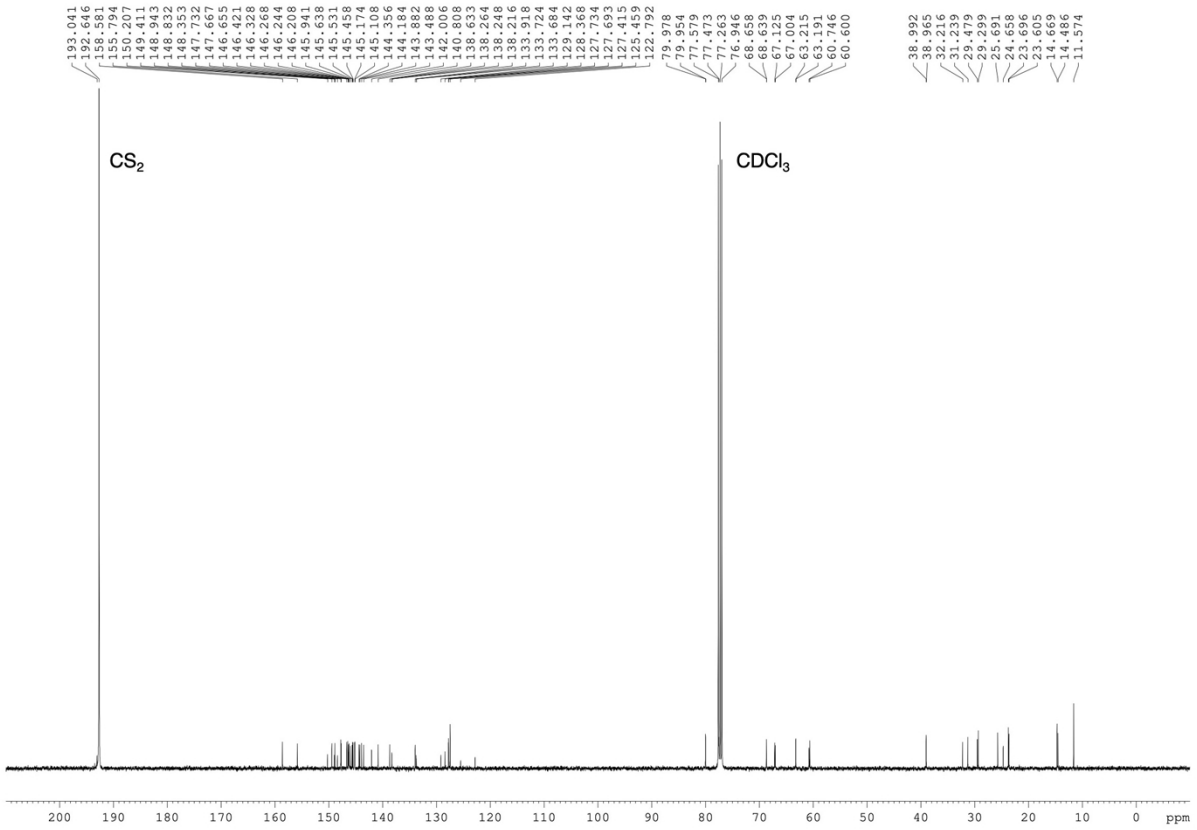

HRMS spectrum (APCI) of **Bis-PC**

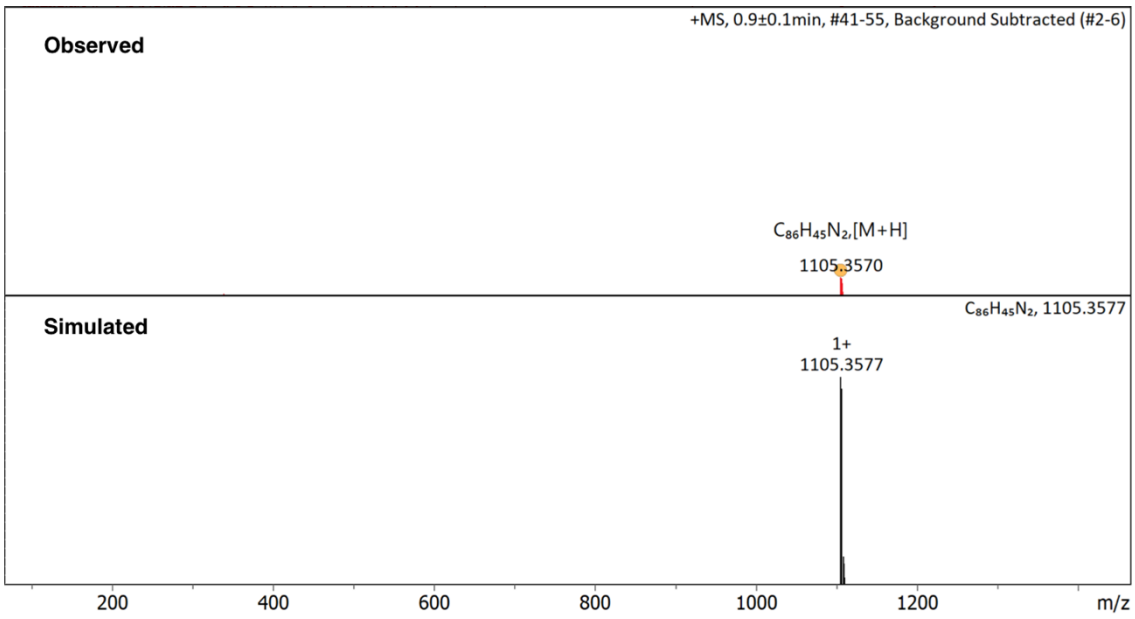

References

[1] H. R. Le Sueur, *J. Chem. Soc., Trans.*, 1910, **97**, 2433.

[2] A. V. Mumyatov, F. A. Prudnov, D. K. Sagdullina, I. V. Martynov, L. N. Inasaridze, A. V. Chernyak, A. V. Maskaev, I. E. Kuznetsov, A. V. Akkuratov and P. A. Troshin, *Synth. Met.*, 2021, **271**, 116632.

[3] Gaussian 16, Revision C.01, M. J. Frisch, G. W. Trucks, H. B. Schlegel, G. E. Scuseria, M. A. Robb, J. R. Cheeseman, G. Scalmani, V. Barone, G. A. Petersson, H. Nakatsuji, X. Li, M. Caricato, A. V. Marenich, J. Bloino, B. G. Janesko, R. Gomperts, B. Mennucci, H. P. Hratchian, J. V. Ortiz, A. F. Izmaylov, J. L. Sonnenberg, D. Williams-Young, F. Ding, F. Lipparini, F. Egidi, J. Goings, B. Peng, A. Petrone, T. Henderson, D. Ranasinghe, V. G. Zakrzewski, J. Gao, N. Rega, G. Zheng, W. Liang, M. Hada, M. Ehara, K. Toyota, R. Fukuda, J. Hasegawa, M. Ishida, T. Nakajima, Y. Honda, O. Kitao, H. Nakai, T. Vreven, K. Throssell, J. A. Montgomery, Jr., J. E. Peralta, F. Ogliaro, M. J. Bearpark, J. J. Heyd, E. N. Brothers, K. N. Kudin, V. N. Staroverov, T. A. Keith, R. Kobayashi, J. Normand, K. Raghavachari, A. P. Rendell, J. C. Burant, S. S. Iyengar, J. Tomasi, M. Cossi, J. M. Millam, M. Klene, C. Adamo, R. Cammi, J. W. Ochterski, R. L. Martin, K. Morokuma, O. Farkas, J. B. Foresman, and D. J. Fox, Gaussian, Inc., Wallingford CT, 2019.

[4] H. Yoshida, *Rev. Sci. Instrum.* 2014, **85**, 016101.

[5] G. M. Sheldrick, SHELX-2018, Program for the Crystal Structure Refinement. University of Göttingen: Göttingen, Germany, 2018.

[6] F. Jahani, S. Torabi, R. Chiechi, L. Koster, J. Hummelen, *Chem. Commun.* 2014, **50**, 10645.

[7] F. Zhao, X. Meng, Y. Feng, Z. Jin, Q. Zhou, H. Li, L. Jiang, J. Wang,Y. Li, C. Wang, *J. Mater. Chem. A* 2015, **3**, 14991.